Tunable Two-Photon Excited Luminescence in Single Gold Nanowires Fabricated by Lithographically Patterned Nanowire Electrodeposition

Hyunmin Kim,[†] Chengxiang Xiang,[†] Aleix G. Güell,[‡] Reginald M. Penner,[†] and Eric O. Potma*,[†]

Department of Chemistry, University of California, Irvine, California 92697-2025, and Department of Physical Chemistry, University of Barcelona, Marti i Franques 1, 08028, Barcelona, Spain

Received: April 15, 2008; Revised Manuscript Received: June 11, 2008

The two-photon excited luminescence (TPEL) of single gold nanowires was investigated under far-field illumination with picosecond pulses. These nanowires, having a rectangular cross-section, a precisely defined thickness, and millimeter-scale length, were prepared by using the lithographically patterned nanowire electrodepostion (LPNE) technique. The TPEL from these wires was investigated as a function of wire thickness. It is found that the optical properties of the wire are dominated by the transverse surface plasmon resonance, which enhances the two-photon absorption process and subsequent emission in the polarization direction of the plasmon mode. Upon tuning the thickness of the wire from 74 to 25 nm, an enhancement of 3 orders of magnitude in the TPEL was observed. The TPEL tunability is found to be consistent with the geometry-dependent field concentration at the metal surface as predicted by the lightning rod model.

1. Introduction

The optical properties of nanostructured gold are largely dictated by the presence of surface plasmons. With strong resonances at optical frequencies, surface plasmons are responsible for the strong absorption bands in the visible range, giving gold nanostructures their typical vivid color. Surface plasmon resonances also dress the surface of the gold nanostructure with locally enhanced electric fields, which have been extensively used for enhancing the otherwise weak optical response of molecules tethered to the metal's surface. These strong surface plasmon enhanced fields render gold nanostructures excellent substrates for surface enhanced Raman scattering (SERS).[1–6]

Besides the linear optical characteristics of gold nanostructures, the nonlinear optical properties of gold nanosystems have also attracted considerable attention. For instance, plasmon resonances enhance the second harmonic generation (SHG) from the metal nanostructure, which can be particularly strong in the case of asymmetries in the nanostructure.[7,8] Third harmonic generation (THG) also benefits from the presence of surface plasmon resonances, which have enabled the observation of strong THG signals from single gold nanospheres.[9] While strongly damped,[10] the surface plasmon resonance facilitates the oscillatory motion of the electrons at optical frequencies, resulting in ample optical nonlinearities. In addition, the strong local fields are expected to boost nonlinear optical signals in the vicinity of the metal's surface. Therefore, gold nanostructures are promising substrates for surface-enhanced coherent anti-Stokes Raman scattering (SE-CARS) studies, a nonlinear analogue of SERS.[11,12] Recent experiments have demonstrated that the optical response at anti-Stokes frequencies of molecules bonded to the gold surface can indeed be enhanced by the plasmon resonances of nanospheres and nanoscopic tips.[11,13]

However, the use of gold nanostructures as antennas for coherent optical nonlinearities is accompanied by an intrinsic photoluminescence of gold.[14] When illuminated with ultrafast radiation, two-photon absorption events in gold give rise to a broad luminescence in the visible range.[15–17] This process is thought to occur through two-photon excitation of d-band electrons to unoccupied sp states of the metal.[18] Subsequent relaxation to the Fermi level results in electron−hole pair recombination under the emission of luminescence. While this photoluminescence is weak for bulk gold, the presence of surface plasmon resonances significantly enhances the two-photon absorption process and the subsequent luminescent emission. The strong luminescence of gold nanostructures has already found applications in biological imaging studies.[17,19]

Understanding the nature of the two-photon excited luminescence (TPEL) is important not only for optimizing the luminescent properties for imaging purposes, but also for finding clues on how to suppress the luminescent background in potential SE-CARS assays. The TPEL background in nonlinear coherent studies of nanostructured gold is substantial, but has not been carefully considered so far.

TPEL has been extensively studied in a variety of structures including nanospheres,[19] nanodisks,[20] and nanorods.[15–17] In particular, the relationship between the plasmon resonance and the luminescent emission in gold nanorods was studied in detail by using near-field optical microscopy. From the polarization dependence of the excitation fields it was concluded that the two-photon absorption is a sequential one-photon absorption process, which is facilitated by the surface plasmon resonance.[16] In addition, the luminescent emission was found to be partially polarized in the direction of the plasmon mode, indicating that the emission process is also plasmon-enhanced.

In this paper we explore the TPEL properties of gold nanostructures further by systematically studying the dependence of the two-photon excited emission on the size of a single plasmon-active nanostructure. We have chosen gold nanowires as our model system because their dimensions can be carefully controlled through the lithographically patterned nanowire electrodeposition (LPNE) technique.[21] The LPNE method produces rectangular nanowires with a precisely defined, na-

* Address correspondence to this author. E-mail: epotma@uci.edu.
[†] University of California.
[‡] University of Barcelona.

10.1021/jp8032758 CCC: $40.75
Published on Web 07/26/2008

nometer-scale thickness and width and a longitudinal axis of millimeters to centimeters. Nanowire geometries have previously been shown to be good SERS substrates.[22] Unlike for the gold nanorods previously studied with near-field microscopy techniques,[15,16] the macroscopic dimension of the long axis of nanowires allows for a direct assessment of plasmon orientation with use of far-field microscopy. Consequently, nanowires enable an accurate correlation of the orientation of the plasmon mode with the polarization dependence of the nonlinear signal in a standard far-field microscope. Furthermore, the nanowires can be studied individually in the absence of internanostructure coupling. While the linear optical properties of gold nanowires prepared with the nanoskyving technique were recently reported,[23] the nonlinear optical properties of nanowire systems have not yet been explored. The goal of this paper is to correlate linear spectroscopy results with the nonlinear optical properties of individual gold nanowires, with a particular emphasis on the magnitude of the optical enhancement as a function of aspect ratio.

Our results indicate that the two-photon absorption process in gold LPNE nanowires is different from that previously observed in gold nanorods. In addition, a strong dependence of the TPEL intensity on the aspect ratio of the wire is found, which is attributed to geometry-dependent local field enhancement of the surface plasmon resonance.

2. Experimental Section

Nanowire Fabrication. The LPNE procedure employed for nanowire fabrication has been previously reported.[21] Briefly, it involved the following seven steps:[21] A glass substrate is cleaned by soaking it in concentrated sulfuric acid and aqueous Nochromix solution overnight. A thin nickel (ESPI 99.999%) film was deposited onto the glass by physical vapor deposition at a rate of 1 Å/s (step 1). Photoresist (Shipley 1808) of 800 nm total thickness was then spin-coated onto the nickel film (step 2). This photoresist was then exposed through a quartz contact mask to 365 nm light for 1.5 min producing a total dose of 0.5 mW/cm^2. The photopatterned sample was subsequently developed in a developer solution (MF 319) for 30 s, rinsed with pure water, and dried in a stream of ultrahigh-purity N_2 (step 3). Then the exposed nickel film was chemically etched in 0.8 M nitric acid until a horizontal trench of width ~500 nm was produced along the perimeter of the photoresist. The total etching time required for the formation of this trench was ~5 min for etching a nickel film of thickness 40 nm (step 4). This trench functions as a template for the formation of a nanowire by electrodepostion in the next step. To effect the electrodeposition of a gold nanowire, the photopatterned and etched surface was immersed in a gold plating solution (6 mM, Clean Earth Inc.) in a three-electrode electrochemical cell. Gold was electrodeposited potentiostatically with use of a computer-controlled potentiostat (Gamry Series G 300) at −0.90 V vs SCE (step 5). Finally, the photoresist was removed by rinsing with acetone (step 6) and the nickel sacrificial layer was dissolved by exposure to dilute (0.7 M) nitric acid for ~15 min (step 7). This LPNE process produced nanowires with a rectangular cross-section characterized by a precisely known (RSD < 5%) thickness (*b*-axis) and a width (*a*-axis) that was known to a precision of 15−20%. The length of these nanowires exceeded 1 mm and these systems are, therefore, quasi-infinite on the nanometer scale. In this study, we have considered three wires of similar width but with different thicknesses: wire A (a = 186 nm, b = 25 nm), wire B (a = 206 nm, b = 48 nm), and wire C (a = 189, b = 74 nm).

Nanowire Characterization. Nanowire thickness and widths were measured with an atomic force microscope (Autoprobe CP, Park Scientific Instruments) operating in noncontact AFM mode. The tips used were V-shaped silicon cantilever (Mikro-Masch Ultrasharp, NC). Figure 1 provides a topographic view of a gold nanowire on glass used for this investigation. The figure clearly shows the rectangular cross-sectional shape of the nanowire, which is continuous along the longitudinal axis of the wire. To ensure the uniformity of the nanowire thickness along its entire length, the AFM profile of each wire was sampled at random along their axes. In addition, cross-sectional profiles of different wires were measured and compared. The statistical variation in the thickness and width of the wires is given in Table 1. Surface roughness of the samples was measured as well, and was determined to be ~4 nm for the background, and ~2 nm for the top of the nanowire.

Laser Scanning Microscopy. Gold nanowire samples are investigated with an inverted laser-scanning microscope (Fluoview 300, Olympus) interfaced with an ultrafast picosecond laser system. The laser light source consists of a mode-locked Nd:Vanadate laser (High-Q Laser, Hohenems, Austria), producing 1064 nm, 10 ps pulses at 76 MHz and with an average power of 10 W, which is used to pump an intracavity doubled optical parametric oscillator (OPO Levante, APE, Berlin, Germany). The OPO delivers ~7 ps pulses that are spectrally tunable in the 770−930 nm range. The radiation of the OPO is combined with part of the 1064 nm radiation on a dichroic mirror and directed to the laser scanning microscope. The tunable radiation from the OPO, here designated as "pump", is the primary source for multiphoton excited photoluminescence in our experiments.

A 695 nm long pass filter was used to cut off any remaining superfluorescence from the light beam before entering the scan head of the microscope. Incident radiation was focused with a high numerical objective onto the sample. A set of objective lenses consisting of 0.65 NA (40×), 0.75 NA (20×), and 1.15W NA (40 ×) was employed in the experiments. Excitation powers at the sample varied from 0.1 to 1.5 mW. Nonlinear signals were collected in the epi-direction and separated from the excitation light with a 760 nm long pass dichroic mirror (Chroma). Signals are detected by either a red-sensitive photomultiplier (R3896 Hamamatsu) through the side port of the microscope or by a grating spectrometer (SpectraPro-150, Acton Research, MA) equipped with a CCD camera (Spec-10, Princeton Instruments, NJ). The emission spectra were spatially averaged by rapidly scanning the focal spot longitudinally over a ~10 μm portion of the wire. Two 650 nm, 40 nm bandwidth bandpass filters (Chroma) were inserted in front of the epi-photomultiplier. Transmission images were obtained simultaneously with the nonlinear contrast images by raster-scanning the focused OPO beam across the sample and detecting the transmitted light with a photomultiplier in the forward direction.

White Light Scattering. Scattering spectra of single nanowires were collected by sending the light of a white light source (HL-2000, Ocean Optics), spatially filtered through a 25 μm pinhole, into the scan head of the microscope. The collimated white light is focused by a 1.15 W NA objective lens onto the nanowire. Scattered light is captured in the epi-direction, separated from the incident light with a 50/50 beamsplitter, and directed onto the grating spectrometer. Similar to the luminescence spectra, scattering spectra were spatially averaged over ~10 μm segments of the wire by rapidly scanning the focal spot along the longitudinal dimension of the wire.

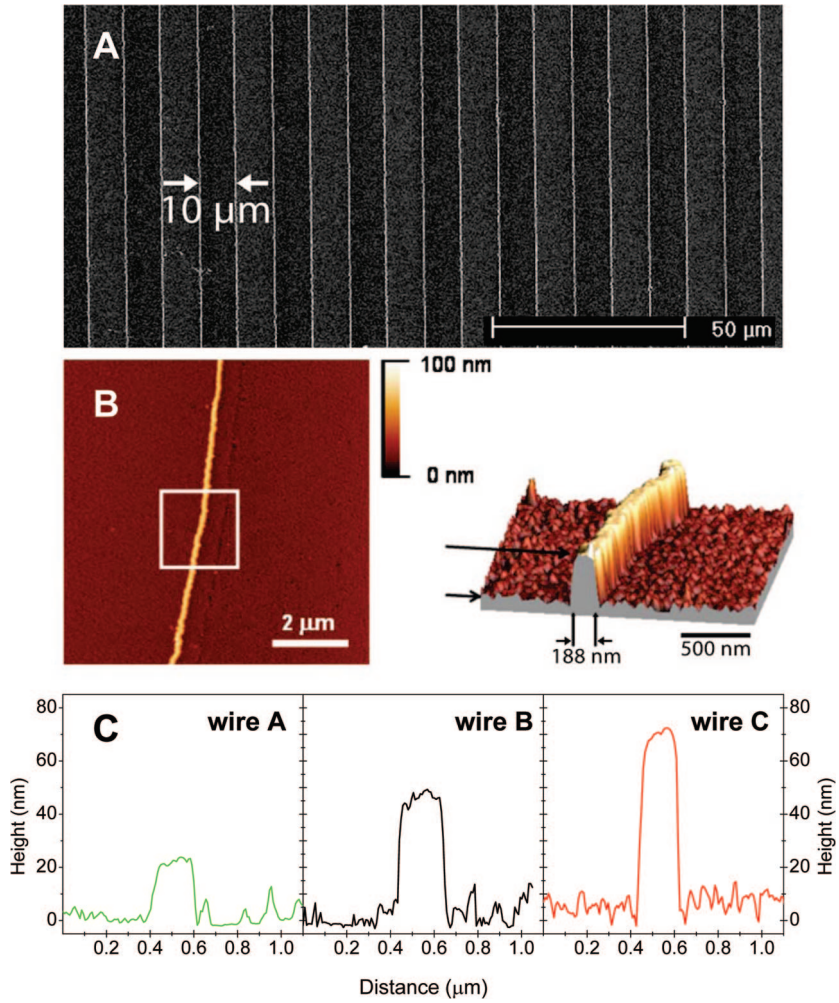

Figure 1. (A) Scanning electron micrograph (SEM) of a gold nanowire array with 10 μm interwire pitch deposited by using the LPNE method. (B) Atomic force microscopy (AFM) topograph of a single gold nanowire with a three-dimensional rendering showing wire dimensions. (C) Cross-sections of three gold nanowires investigated in this study showing wire width and height dimensions.

TABLE 1: Statistical Data of Thickness and Width for the Three Different Samples

wire	thickness (nm)	width (nm)	aspect ratio
A	25.4 ± 1	186 ± 15	7.35
B	47.8 ± 3	206 ± 23	4.28
C	73.8 ± 3	189 ± 17	2.56

3. Linear Response

We have studied the linear scattering properties of single nanowires to gain insight in the spectral location of the nanostructure's transverse surface plasmons. To mimic the nonlinear excitation conditions in terms of the angle of incidence of the incoming light, we use the same high numerical objective for the light-scattering experiments. Figure 2a shows a schematic diagram of the focused incident beam geometry. The incoming light is linearly polarized and collimated, resulting in an illumination spot at the nanowire of only a few micrometers in diameter. When the incoming light is polarized along x, the majority of the focal field components are x-polarized. However, a small portion of the focal intensity distribution, about 1% relative to the x-polarized intensity, is polarized in the z-direction.[24] In principle, when the a-axis of the nanowire is aligned with the incoming x-polarization, both transverse surface plasmon modes oriented along the a and b direction are excited, albeit with significantly different excitation efficiencies. In our excitation and collection geometry, the scattering spectra are dominated by the transverse surface plasmon resonance along the a-axis of the nanowire.

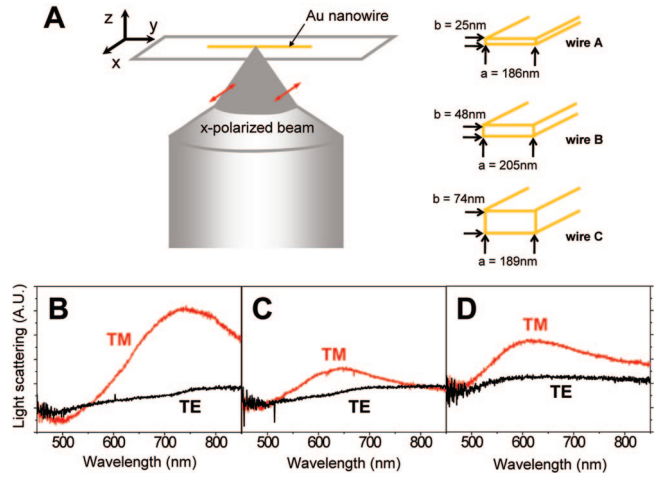

Figure 2. (A) Excitation geometry for x-polarized incident beam illumination of nanowires. Panels B, C, and D show the white light scattering spectra of wire A ($r = a/b = 7.35$), wire B ($r = 4.28$) and wire C ($r = 2.56$) gold nanowires, respectively. TM denotes the situation when the incident beam is perpendicularly polarized to the longitudinal axis of the wire and TE when it is parallel. Signal integration time was 50 s.

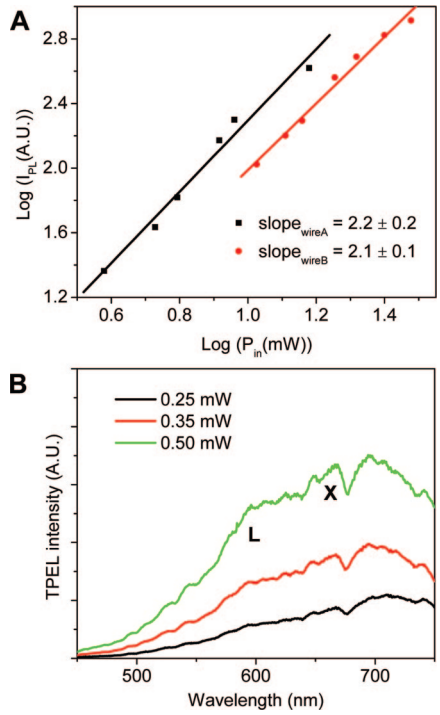

Figure 3. (A) Power dependence of TPEL for wires A and B. Solid lines are fits to the data. (B) Power dependence of the TPEL emission spectrum of wire A. X and L mark the spectral location of the corresponding symmetry points of the first Brillioun zone of Au.

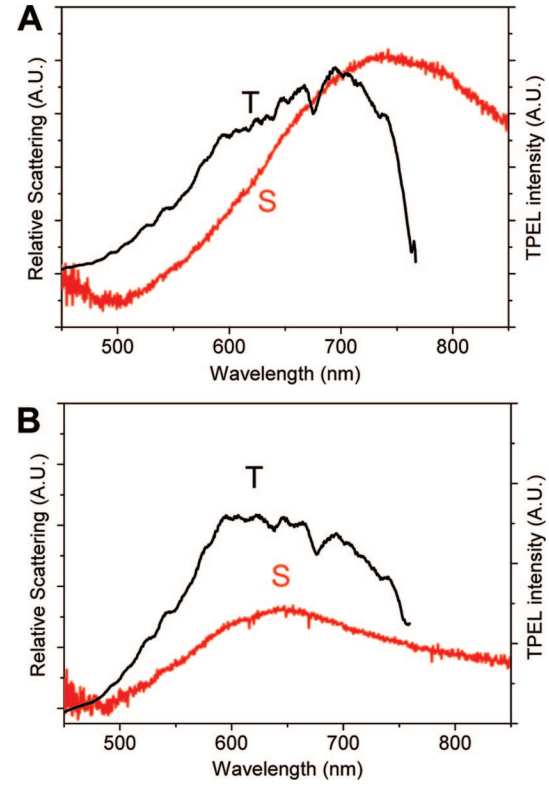

Figure 4. Overlap plots of TPEL and SPR scattering spectra for (A) wire A and (B) wire B. T corresponds to TPEL; S labels the white light scattering spectrum.

The white light scattering spectrum from a single wire of type A is shown in Figure 2b. When the incident light is polarized parallel to the *a*-axis of the wire, a broad scattering spectrum is observed that peaks around 740 nm. Such broad scattering spectra have been observed before in gold and silver nanowires and may reflect strong plasmon damping in the nanowires combined with spatially varying plasmon absorption along the wire.[23,25,26]

Upon increasing the thickness of the wire, the scattering spectrum shows an effective blue shift, as shown in parts c and d of Figure 2. A similar spectral dependence has been reported for silver nanowires,[25] which is consistent with the general trend of shorter plasmon resonance wavelengths for smaller aspect ratios of the nanostructure.

The spectral signatures are significantly less prominent when the incident light is polarized along the longitudinal direction of the wire. Because the longitudinal mode is not a localized plasmon mode, no significant surface plasmon related absorption in the visible range is expected.

4. Two-Photon Excited Luminescence Spectrum of Individual Wires

Excitation of the nanowires with ultrafast pulses in the 780−820 nm range produces a broad luminescence spectrum. For all wires examined, the emission intensity scales to the second order with the power of the incident light (Figure 3a), indicating that the emission is the result of a two-photon excitation process. The single wire spectral profile is independent of the fluence used in our experiments, as shown in Figure 3b.

The spectral dip at 675 nm is reproducible and is independent of our instrument's spectral sensitivity. Shallow spectral bumps can be recognized at 660 and 590 nm, which are reminiscent of emission resulting from electron−hole radiative recombination at the X and L symmetry points, as previously observed in gold crystalline nanorods.[16] The gold nanowires studied here are polycrystalline, and the lack of structure in the observed emission spectrum is attributed to the loss of a well-defined lattice symmetry in the gold wire.

The emission spectrum is shaped not only by the radiative states of the gold but also by the surface plasmon-assisted field enhancement. Figure 4 compares the scattering spectrum with the emission spectrum of wire A (panel a) and wire B (panel b). The emission spectrum of wire A is red-shifted relative to that of the photoluminescence spectrum of wire B. The shift in the emission correlates well with the spectral location of the surface plasmon as measured with the scattering spectrum. The transverse surface plasmons of the nanowire thus selectively enhance part of the gold luminescence spectrum.

5. Size Dependence

Figure 5 shows TPEL images of single gold nanowires with different aspect ratios. All wires studied exhibited clear two-photon excited luminescence. Within a single wire, variations in the luminescence intensity at different positions along the wire are seen. We attribute these variations to local irregularities of the wire. In the following, to reliably compare the TPEL response as a function of wire dimension, we have taken the average signal of wire segments, each at least 25 μm long.

At an excitation wavelength of 780 nm, strong TPEL signal is observed from wire A (b = 25 nm). As the thickness of the wire is increased from 25 to 75 nm, the TPEL response decreases by almost 3 orders of magnitude. Upon tuning the excitation wavelength 817 nm, a clear decrease of the TPEL intensity is seen. For the wires studied here, such a decrease is expected as scattering spectra predict a more efficient driving of the transverse surface plasmon at the shorter excitation wavelength.

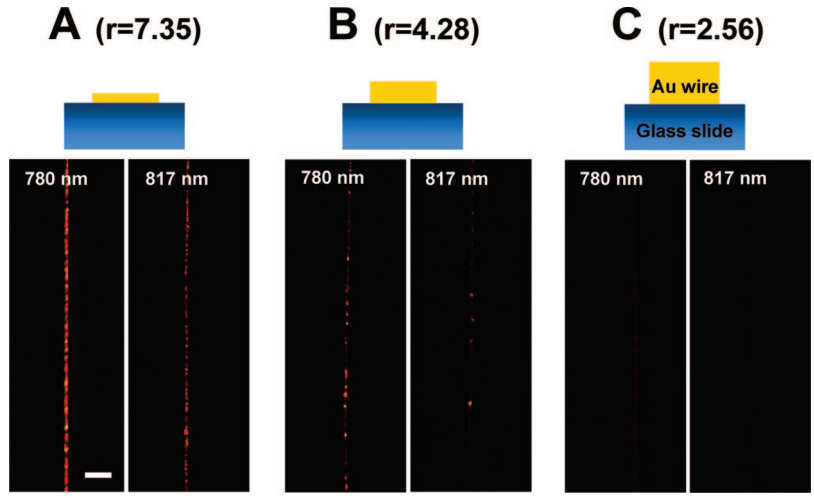

Figure 5. TPEL images of (A) wire A, (B) wire B, and (C) wire C excited by 780 and 817 nm, respectively. For all measurements 1 mW of power is used. The incident beam is polarized along the short axis of the wire. The scale bar corresponds to 5 μm.

A simple model based on the lightning rod effect can be used to qualitatively understand the TPEL dependence on the aspect ratio of the nanowire. The TPEL intensity can be approximated by:[18,27]

$$I_{\mathrm{TPEL}} \approx [L(\omega_p)]^4[L(\omega_{\mathrm{PL}})]^2 \quad (1)$$

where $L(\omega_p)$ and $L(\omega_{\mathrm{PL}})$ are the local field correction factor for the incident pump field and the emitted fields, respectively. In the lightning rod model, the local field correction factor is factored into a material dependent surface plasmon correction factor $L_{\mathrm{sp}}(\omega)$ and a lightning rod factor L_{LR}, which depends on the aspect ratio (a,b) of the nanostructure alone:[28–30]

$$L(\omega) = L_{\mathrm{sp}}(\omega)L_{\mathrm{LR}} \quad (2)$$

The lightning rod factor describes the concentration of the field as function of geometry, and plays an important role in determining the magnitude of the optical enhancement. Analytical expressions for the local field correction factor can be obtained if the nanostructure is modeled as an elliptical spheroid. Such an approximation is reasonable for the case of nanorods, but is less appropriate for modeling rectangular nanowires. Nonetheless, the physics of the concentration of local fields, due to compression along one of the axes of the nanostructures, is effectively captured by the changing aspect ratio of the elliptical spheroid. Therefore, we will employ the elliptical model to gain insight into the enhancement of the wire as a function of thickness. Within this assumption, the local field correction factors are written as:[18]

$$L_{\mathrm{sp}}(\omega) = \left[\varepsilon_m(\omega) - 1 + \frac{1}{A}\left\{1 + i\frac{4\pi^2 V}{3\lambda^3}(1 - \epsilon_m(\omega))\right\}\right]^{-1}$$
$$L_{\mathrm{LR}} = 1/A \quad (3)$$

where ω is the photon frequency, $\varepsilon_{\mathrm{m}}(\omega)$ is the complex dielectric functions of the metal, V is the volume of the nanostructure that is illuminated, and λ is the wavelength of the incident light. With the laser light polarized along the a-axis of the wire, the depolarization factor A is given as:[30]

$$A = \frac{ab^2}{2}\int_0^\infty \frac{ds}{(s+a^2)^{3/2}\cdot(s+b^2)} \quad (4)$$

Indeed, we find qualitative agreement between our data and the trend predicted by the lightning rod correction factor through eqs 1–4. Figure 6a shows the results of the calculated relative TPEL as a function of the thickness of the wire within this simple model. For a fixed width of a, maximum TPEL signals are predicted for nanowires of thickness ~30 nm. The calculation indicates that when the thickness of the wire is increased by a factor of 2, the TPEL signal decreases by 3 orders of magnitude. The predicted relative enhancement is corroborated by the experimental results as summarized in Figure 6b. The decreasing TPEL signal with wire thickness is correctly reproduced, as well as the spectral dependence of the plasmon local field enhancement.

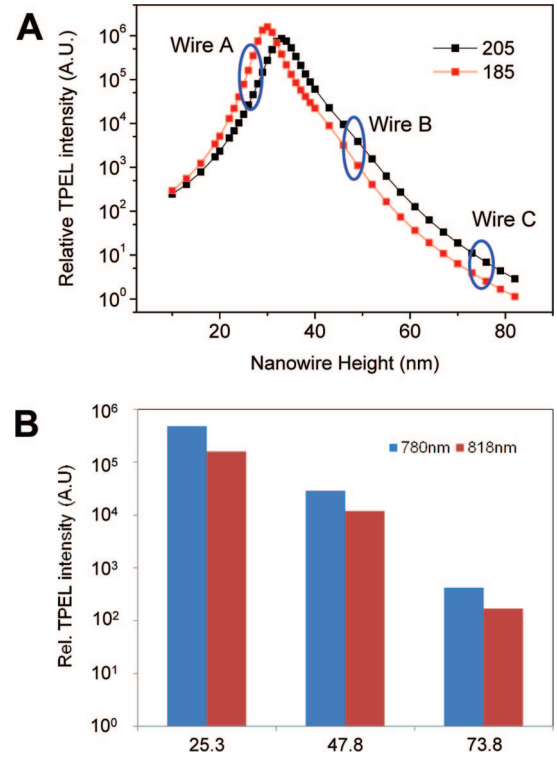

Figure 6. (A) Relative TPEL intensity calculated based on the lightning rod model. The calculation is performed as a function of nanowire height, for two fixed widths (185 and 205 nm) and 780 nm excitation. Marked points indicate heights for the three nanowires studied here. (B) Relative TPEL intensities for two different wavelengths of excitation beams. Wires are indicated by their height (in nm).

Strongest TPEL signals are thus observed when the laser excitation maximally overlaps with the surface plasmon reso-

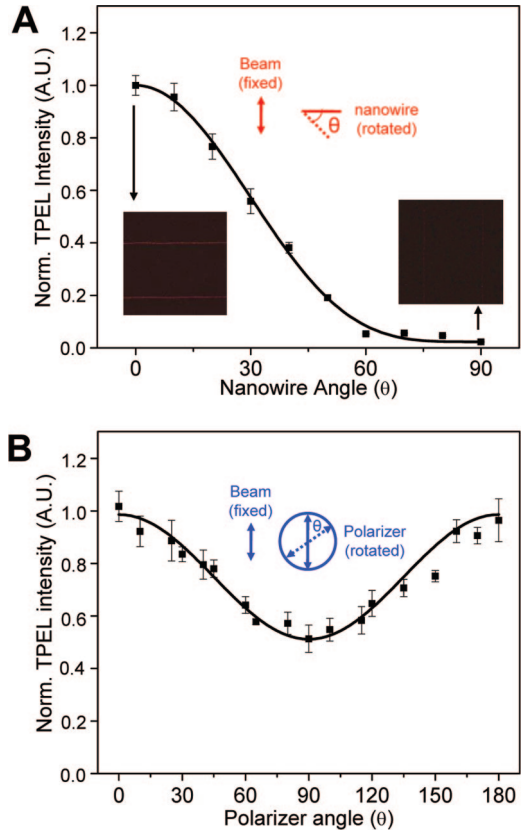

Figure 7. (A) Excitation polarization dependence of TPEL for wire A. The insets in panel A are TPEL images taken when the angles are 0° and 90°, respectively. (B) Polarization dependence of emission for wire A. The incident power at 780 nm was 0.4 mW.

nance frequency and when the aspect ratio of the wire is close to $a/b \approx 6.5$, which ensures maximum concentration of the local fields. The lithographic patterning of the nanowires allowed for maximum flexibility in adjusting the wire's dimensions for optimizing the optical enhancement.

6. Polarization Dependence

The unique geometry of the LPNE nanowires allows us to clearly identify the orientation of the active plasmon mode. When the excitation light is polarized along the transverse surface plasmon mode in the *x*-direction, a strong TPEL response is observed. In contrast, when the excitation light is orthogonally polarized to the surface plasmon, the TPEL signal decreases by several orders of magnitude. The TPEL signal as a function of the angle θ between the longitudinal axis of the wire and the polarization of the excitation light is shown in Figure 7a. A clear $\sin^4 \theta$ dependence is seen, which corroborates the previously observed excitation polarization dependence of dumbbell shaped nanorods.[17] This is in contrast, however, with results obtained from crystalline gold nanorods, where a $\sin^2 \theta$ dependence was found that provided evidence for a sequential incoherent two-photon absorption process.[16] The TPEL polarization dependence of gold nanowires is similar to the SHG polarization dependence previously observed in nanorods.[16] This finding suggests that a two-step absorption process is not essential to explain the TPEL in nanowires. Indeed, similar to the instantaneous coherent interaction of two photons in SHG, the two-photon absorption process observed in gold nanowires most probably involves the instantaneous absorption of two photons.

Unlike the clear excitation polarization dependence, the emission is only partially polarized. This indicates that not all the emission contributions are resonantly coupled to the surface plasmon mode for maximum enhancement. Nonetheless, polarized components align well with the direction of the transverse plasmon mode, which hints at a possible role of the surface plasmon in emission enhancement. Such plasmon-enhanced emission is in agreement with the plasmon-induced shifts in the luminescence spectra as discussed in Figure 4.

7. Conclusion

In this work, we have demonstrated strong TPEL of rectangular gold nanowires. The well-defined geometry of the lithographically patterned nanowire allowed us to study the magnitude of the TPEL emission as a function of wire thickness. The TPEL intensity was found to be tunable over 3 orders of magnitude by varying the wire thickness in a controlled fashion from 25 to 74 nm. Such controlled tunability permitted a careful optimization of the local field enhancement. Because of the semi-infinite longitudinal axis of the LPNE gold nanowire, we were able to use far-field microscopy to study the polarization dependence of the field enhancement. From these measurements, we determined that the two-photon absorption in gold nanowires is probably an instantaneous process rather than a sequential incoherent absorption of two photons.

In designing assays for SE-CARS based on gold nanostructures, the strong TPEL background imposes a challenge. Future SE-CARS applications will not only have to focus on optimization of local field enhancement, but will also need to incorporate a careful management of these luminescent contributions.

Acknowledgment. We thank Prof. Ara Apkarian for providing the CCD camera used in this study, and for helpful discussions. E.O.P. acknowledges support from the American Chemical Society (PRF 46067-G6). Part of this research is supported by the National Science Foundation, Chemical Bonding Center, Grant CHE-0533162. R.M.P. acknowledges financial support from the National Science Foundation, Grant CHE-0641169.

References and Notes

(1) Moskovits, M. Surface-enhanced spectroscopy. *Rev. Mod. Phys.* **1985**, *57*, 783–826.

(2) Kneipp, K.; Dasari, R. R.; Wang, Y. Near-infrared surface-enhanced Raman scattering (NIR SERS) on colloidal silver and gold. *Appl. Spectrosc.* **1994**, *48*, 951–955.

(3) Lee, P. C.; Meisel, D. Absorption and surface-enhanced Raman of dyes on silver an gold sols. *J. Phys. Chem.* **1982**, *86*, 3391–3395.

(4) Otto, A.; Mrozek, I.; Grabborn, H.; Akermann, A. Surface-enhanced Raman scattering. *J. Phys.: Condens. Matter* **1992**, *4*, 1143–1212.

(5) Nie, S.; Emory, S. R. Probing single molecules and single nanoparticles by surface-enhanced Raman scattering. *Science* **1997**, *275*, 1102–1106.

(6) Dieringer, J. A.; Lettan, R. B.; Scheidt, K. A.; Duyne, R. P. V. A frequency-domain proof of single molecule surface-enhanced Raman spectroscopy. *J. Am. Chem. Soc.* **2007**, *129*, 16249–16256.

(7) Antoine, R.; Brevet, P. F.; Girault, H. H.; Bethell, D.; Schiffrin, D. Surface plasmon enhanced non-linear optical response of gold nanoparticles at the air-toluene interface. *Chem. Commun.* **1997**, (19), 1901–1902.

(8) Bouhelier, A.; Beversluis, M.; Hartschuh, A.; Novotny, L. Near-field second-harmonic generation induced by local field enhancement. *Phys. Rev. Lett.* **2003**, *90*, 013903.

(9) Lippitz, M.; Dijk, M. A. v.; Orrit, M. Third-harmonic generation from single gold nanoparticles. *Nano Lett.* **2005**, *5*, 799–802.

(10) Pelton, M.; Liu, M.; Park, S.; Scherer, N. F.; Guyot-Sionnest, P. Ultrafast resonant optical scattering from single gold nanorods: Large nonlinearities and plasmon saturation. *Phys. Rev. B* **2006**, *73*, 155419.

(11) Ichimura, T.; Hayazawa, N.; Hashimoto, M.; Inouye, Y.; Kawata, S. Tip-enhanced coherent anti-Stokes Raman scattering for vibrational nanoimaging. *Phys. Rev. Lett.* **2004**, *92*, 220801.

(12) Koo, T. W.; Chan, S.; Berlin, A. A. Single-molecule detection of biomolecules by surface-enhanced coherent Raman scattering. *Opt. Lett.* **2005**, *30*, 1024.

(13) Ichimura, T.; Hayazawa, N.; Hashimoto, M.; Inouye, Y.; Kawata, S. Local enhancement of coherent anti-Stokes Raman scattering by isolated gold nanoparticles. *J. Raman Spectrosc.* **2003**, *34*, 651–654.

(14) Beversluis, M. R.; Bouhelier, A.; Novotny, L. Continuum generation from single gold nanostructures through near-field mediated intraband transitions. *Phys. Rev. B* **2003**, *68*, 115433.

(15) Bouhelier, A.; Bachelot, R.; Lerondel, G.; Kostcheev, S.; Royer, P.; Wiederrecht, G. P. Surface plasmon characteristics of tunable photoluminescence in single gold nanorods. *Phys. Rev. Lett.* **2005**, *95*, 267405-4.

(16) Imura, K.; Nagahara, T.; Okamoto, H. Near-field two-photon induced photoluminscence from single gold nanorods and imaging of plasmon modes. *J. Phys. Chem. B* **2005**, *109*, 13214–13220.

(17) Wang, H.; Huff, T. B.; Zweifel, D. A.; He, W.; Low, P. S.; Wei, A.; Cheng, J.-X. In vitro and in vivo two-photon luminescence imaging of single gold nanorods. *Proc. Natl. Acad. Sci. U.S.A.* **2005**, *102*, 15752–15756.

(18) Boyd, G. T.; Yu, Z. H.; Shen, Y. R. Photoinduced luminescence from the noble metals and its enhancement on roughened surfaces. *Phys. Rev. B* **1986**, *33*, 7923–7936.

(19) Farrer, R. A.; Butterfield, F. L.; Chen, V. W.; Fourkas, J. T. Highly efficient multiphoton-absorption-induced luminescence from gold nanoparticles. *Nano Lett.* **2005**, *5*, 1139–1142.

(20) Imura, K.; Nagahara, T.; Okamoto, H. Photoluminescence from gold nanoplates induced by near-field two-photon absorption. *Appl. Phys. Lett.* **2006**, *88*, 023104.

(21) Menke, E. J.; Thompson, M. A.; Xiang, C.; Yang, L. C.; Penner, R. M. Lithographically patterned nanowire electrodeposition. *Nature Mat.* **2006**, *5*, 914–919.

(22) Billot, L.; Chapelle, M. L. d. l.; Grimault, A. S.; Barschiesi, V. A. D.; Bijeon, J. L.; Adam, P. M.; Royer, P. Surface enhanced Raman scattering on gold nanowire arrays: evidence of strong multipolar surface plasmon resonance enhancement. *Chem. Phys. Lett.* **2006**, *422*, 303–307.

(23) Xu, Q.; Bao, J.; Capasso, F.; Whitesides, G. M. Surface plasmon resonances of free-standing gold nanowires fabricated using nanoskiving. *Angew. Chem.* **2007**, *1108*, 3713–3717.

(24) Richards, B.; Wolf, E. Electromagnetic diffraction in optical systems II. Structure of the image field in an aplanatic system. *Proc. R. Soc. Londen, Ser. A* **1959**, *253*, 358–379.

(25) Krenn, J. R.; Schider, G.; Rechberger, W.; Lamprecht, B.; Leitner, A.; Aussenegg, F. R.; Weeber, J. C. Design of multipolar excitations in silver nanoparticles. *Appl. Phys. Lett.* **2000**, *77*, 3379–3381.

(26) Schider, G.; Krenn, J. R.; Hohenau, A.; Ditlbacher, H.; Leitner, A.; Aussenegg, F. R.; Schaich, W. L.; Puscasu, I.; Monacelli, B.; Boreman, G. Plasmon dispersion relation of Au and Ag nanowires. *Phys. Rev. B* **2003**, *68*, 155427–155424.

(27) Chen, C. K.; Heinz, T. F.; Ricard, D.; Shen, Y. R. Surface-enhanced second-harmonic generation and Raman scattering. *Phys. Rev. B* **1983**, *27*, 1965–1979.

(28) Boyd, G. T.; Rasing, T.; Leite, J. R. R.; Shen, Y. R. Local-field enhancement on rough surfaces of metals, semimetals, and semiconductors with the use of optical second-harmonic generation. *Phys. Rev. B* **1984**, *30*, 519–525.

(29) Gersten, J.; Nitzan, A. Electromagnetic theory of enhanced Raman scattering by molecules adsorbed on rough surfaces. *J. Chem. Phys.* **1980**, *73*, 3023–3037.

(30) Liao, P. F.; Wokaun, A. Lightning rod effect in surface enhanced Raman scattering. *J. Chem. Phys.* **1982**, *76*, 751–752.

JP8032758